Available online at www.sciencedirect.com
SCIENCE DIRECT®
ELSEVIER
Applied Surface Science 210 (2003) 128–133
applied surface science
www.elsevier.com/locate/apsusc

KPFM imaging of Si(1 1 1)$5\sqrt{3} \times 5\sqrt{3}$-Sb surface for atom distinction using NC-AFM

Kenji Okamoto[a,*], Kentaro Yoshimoto[b], Yasuhiro Sugawara[c,d], Seizo Morita[b,d]

[a]*Low Temperature Center, Osaka University, 2-1 Yamada-oka, Suita, Osaka 565-0871, Japan*
[b]*Department of Electronic Engineering, Graduate School of Osaka University, 2-1 Yamada-oka, Osaka 565-0871, Japan*
[c]*Department of Applied Physics, Graduate School of Osaka University, 2-1 Yamada-oka, Suita, Osaka 565-0871, Japan*
[d]*Handai Frontier Research Center, Osaka University, 2-1 Yamada-oka, Suita, Osaka 565-0871, Japan*

Abstract

We investigate the possibility of distinction of individual atom species using noncontact atomic force microscopy (NC-AFM) combined with the electrostatic force (ESF) measurement. We simultaneously measured the topography and the surface potential on the Si(1 1 1)$5\sqrt{3} \times 5\sqrt{3}$-Sb surface by Kelvin probe force microscopy (KPFM). The surface potential image indicates the existence of two kinds of adatoms while the difference is not clear in topography. Atom species of each adatom are specified from other NC-AFM images with different experimental conditions and therefore spots with a lower surface potential are specified as Si adatoms. It is found that, in addition to adatoms, Si rest atoms can be specified from the surface potential image. The result indicate that KPFM has the ability to distinguish the individual atom species on intermixing surfaces.

PACS: 61.16.Ch; 68.35.Bs

Keywords: Noncontact atomic force microscopy (NC-AFM); Electrostatic force measurement; Kelvin probe force microscopy (KPFM); Atomic resolution; Atom distinction

Noncontact atomic force microscopy (NC-AFM) has achieved the true atomic resolution in observation of surface structures of Si(1 1 1)7 × 7 [1,2] and InP(1 1 0) [3] in 1995. Recently, identification of individual atoms is desired for better understanding of surface science or further application of NC-AFM, such as single atom manipulation. NC-AFM, as well as scanning tunneling microscopy (STM), has shown to have the possibility to specify the species of individual atoms under limited conditions. In the case of NC-AFM, the knowledge of the surface structure is required for specification from topography, then, e.g., the sample must be a well-known reconstructed surface. The possibility of atom distinction due to comparison of images with different kinds of tips [4] has been shown, but it is still difficult to completely control tip-apex atoms. In the case of STM, there is an advantage that STM can extra information for individual atoms in addition to surface structure, such as energy-state structure, using tunneling spectroscopy measurement, e.g. However, STM has a disadvantage that the sample must be conductive. We paid attention to the electrostatic force (ESF) measurement,

* Corresponding author.
E-mail address: okamoto@ele.eng.osaka-u.ac.jp (K. Okamoto).

0169-4332/03/$ – see front matter
doi:10.1016/S0169-4332(02)01492-7

which can be expected to add an extra information to NC-AFM observations.

For the ESF measurement using AFM, Kelvin probe force microscopy (KPFM) has been developed [5]. KPFM detects the ESF arising from the contact potential difference (CPD) between the tip and the sample, and hence has the ability to observe the spatial distribution of surface potential with high resolution of NC-AFM [6,7]. Its resolution has been improved with that of NC-AFM, and atomic resolution has been already achieved [8,9]. We employed this technique of the ESF measurement on atomic scale and tried distinction of atoms on Sb/Si intermixing surfaces.

When Sb is deposited on Si(1 1 1) surfaces with less than 1 ML coverage, various structures can be formed depending on the coverage and annealing temperature. Especially, we are interested in the $5\sqrt{3} \times 5\sqrt{3}$ reconstructed structure because both Si and Sb adatoms coexist on it. The detailed study of the $5\sqrt{3} \times 5\sqrt{3}$ structure and the formation process during annealing were recently reported by Saranin et al. [10] using STM. According to STM observation, there is little difference in topography between Si and Sb adatoms and the distinction of those was a problem to be discussed. In 1999, Ko et al. [11] calculated and claimed that Si adatoms were imaged as dim spots in empty-state images and their prediction was proved by experimental results obtained later [10,11]. From those experiments, it was confirmed that Si and Sb adatoms coexist on Si(1 1 1)$5\sqrt{3} \times 5\sqrt{3}$-Sb surfaces.

In this paper, we report the KPFM measurement on the Si(1 1 1)$5\sqrt{3} \times 5\sqrt{3}$-Sb surface using KPFM with atomic resolution. In our knowledge, this experiment is first attempt to identify species of individual atoms by ESF measurement. We expect that Si and Sb adatoms can be distinguished due to the difference in electrical property, such as work function, ionization energy, electronegativity, or the local distribution of electron density.

When Sb is deposited on the Si(1 1 1) surface with less than 1 ML coverage, various structures can be made depending on coverage and annealing temperature [12–15]. After deposition of ~1 ML and annealing at ~630 °C, the 2 × 1 structure is formed [14–16]. Subsequent annealing at ~700 °C forms the $5\sqrt{3} \times 5\sqrt{3}$ structure [10,14,16]. Si(1 1 1)$5\sqrt{3} \times 5\sqrt{3}$-Sb surfaces has been investigated principally by STM [10,14,16,17]. The ideal structure model with boundary

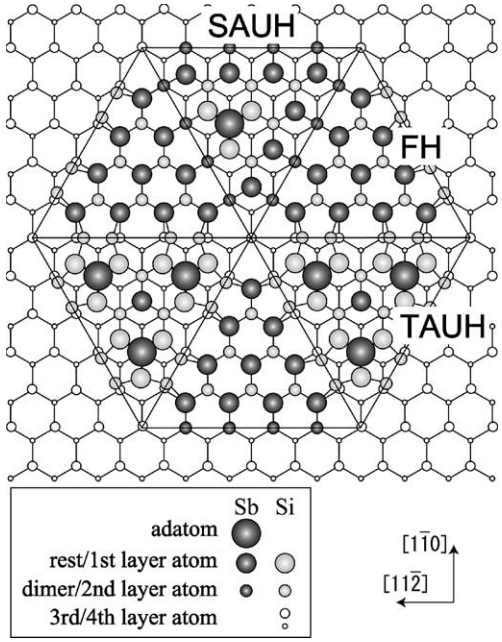

Fig. 1. Ideal structure model of the Si(1 1 1)$5\sqrt{3} \times 5\sqrt{3}$-Sb surface as proposed by Saranin et al. [10].

Sb atoms is proposed by Saranin et al. [10] as shown in Fig. 1. The unit cell consists of faulted subunits and two kinds of unfaulted subunits which are labeled as faulted half (FH), triple-adatoms unfaulted half (TAUH) and single-adatom unfaulted half (SAUH), respectively, following the notation of Park et al. [16]. On FH, there are 10 Sb rest atoms which replaced Si rest atoms. Two-third of unfaulted subunits are TAUH, which have three Sb adatoms, and the others are SAUH, which have single Sb adatom. On TAUHs and SAUHs, each Sb adatom is coupled with three Si rest atoms, while the other rest atoms are Sb. According to papers [10,11,14,16] and our experience, there are numbers of defects on $5\sqrt{3} \times 5\sqrt{3}$ surfaces, i.e. there are numbers of extra or lost adatoms and a part of Sb adatoms are replaced by Si atoms. As a result, an Sb/Si intermixing surface is usually formed.

We prepared the sample as follows. At first, we prepared the clean Si(1 1 1)7 × 7 reconstructed surface. Then a few MLs of Sb were deposited on the Si surface using an evaporator, which can monitor and control the deposition rate. During the deposition, the Si substrate was heated at 630 °C. The heating was kept for ~10 min after deposition to form the 2 × 1

structure. We observed the sample surface by low energy electron diffraction (LEED) and confirmed that the 2×1 structure was surely formed. The subsequent annealing at 700 °C for 1 min was done to form the $5\sqrt{3} \times 5\sqrt{3}$ structure. The $5\sqrt{3} \times 5\sqrt{3}$ structure was confirmed by LEED observation [12]. The procedure of deposition and annealing was done in ultrahigh vacuum ($P \leq 5 \times 10^{-10}$ Torr).

We made KPFM measurements using a homemade NC-AFM/KPFM system [9]. We used Sb-doped Si cantilever with the bare Si tip, the oxidized layer and contamination on which were removed by Ar-ion bombardment. The resonance frequency, the spring constant, the oscillation amplitude of the cantilever were 167 kHz, 35 N/m, 102 Å, respectively. The frequency shift is −29 Hz and the scan size is 121× 85 Å^2. AC electric field with frequency of 1 kHz and amplitude of 1 V_{rms} was applied between the tip and the sample for KPFM. The simultaneously measured topography, the cross section at the white solid line on topography and CPD image are shown in Fig. 2(a)–(c), respectively. Adatoms of the $5\sqrt{3} \times 5\sqrt{3}$ structure can be seen as bright spots in Fig. 2(a), although periodicity is not complete. A hexagon indicates one of unit cells, which corresponds to the one shown in Fig. 1, as an example. There are six adatoms on TAUHs and an adatom on SAUH. Four extra adatoms, which should not exist on ideal structure, can be seen on FHs. In the CPD image, the image contrast is inverted against the topography, i.e. adatoms are imaged as black spots. It can be seen that there are two kinds of adatoms, i.e. there is a slight height difference in the topography, and an obvious potential difference in CPD image. We thought those difference is due to the difference of atom species. Fig. 2(b) includes the five adatoms including both kinds. We evaluated the difference in the average peak height of two kinds of adatoms from the peak height of each adatom, and obtained the value of 0.29 ± 0.17 Å.

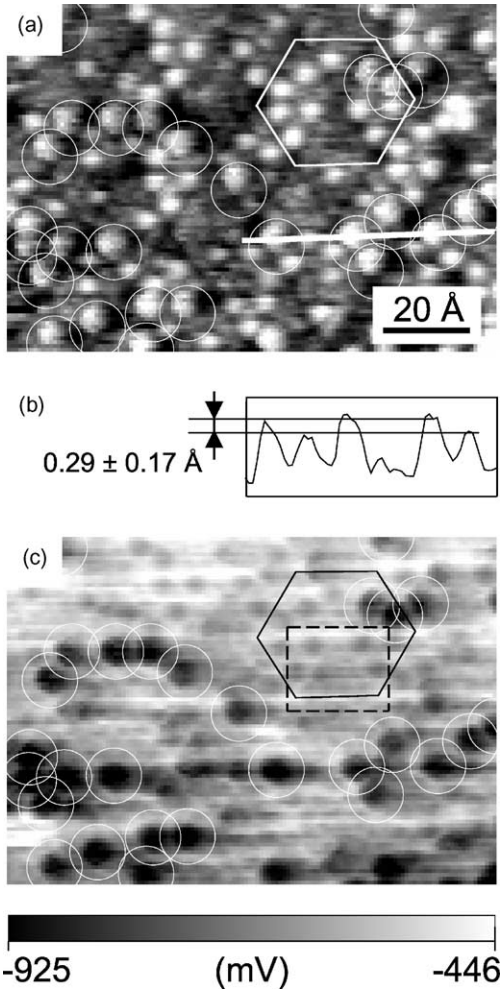

Fig. 2. Topography (a), the cross section at the white solid line on the topography (b), and the CPD (c) image obtained with NC-AFM/KPFM are shown. The frequency shift is −29 Hz and the scan size is 121 × 85 Å^2. In (a) and (c), there can be seen two kinds of adatoms. (b) Includes five adatoms of both kinds. The difference in the average peak height between two kinds is 0.29 ± 0.17 Å.

We have found that we can specify which is a Si and a Sb adatom, respectively, from NC-AFM images with different tip-apex atoms [4]. Fig. 3 shows the obtained topographies. The experimental conditions are almost the same as in the KPFM measurement except that the bias voltage is not applied between the tip and the sample. The scan areas of the two images are the same (241 × 241 Å^2) except for the slight thermal drift. The frequency shift was kept to be −36 Hz in Fig. 3(a) and −22 Hz in Fig. 3(b). The cross sections at the solid lines, the position of which correspond to that of the line in Fig. 2(a), are also shown. The differences in the average peak height of two kinds of adatoms are 0.56 ± 0.23 and 0.30 ± 0.21 Å, respectively. We can see that the image contrast is obviously enhanced between both scans. Fig. 3(b) resolves much more adatoms, which appear as white spots, than (a). Fig. 3(a) also has the atomic resolution because some of the adatoms are individually resolved. It is notable

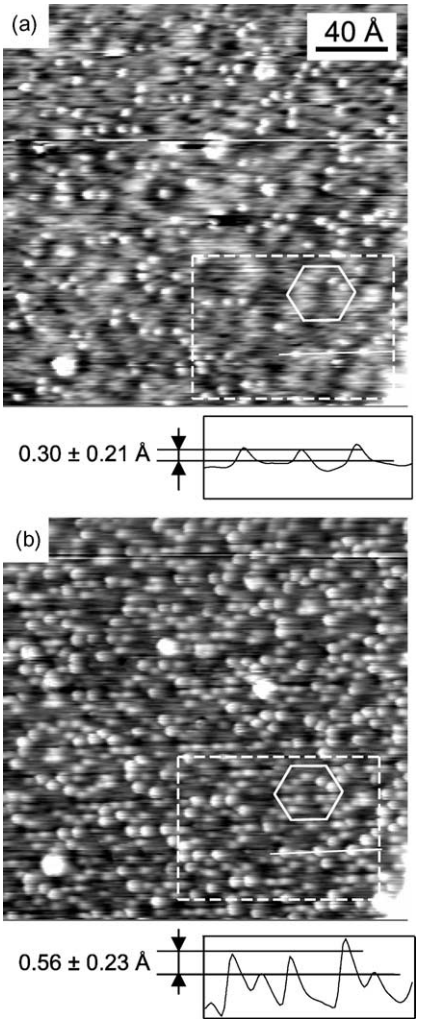

Fig. 3. Topography observed with an (a) Sb and (b) Si tip-apex atoms. The resonance frequency and the spring constant of the cantilever are 167 kHz and 35 N/m, respectively. The oscillation amplitude is 102 Å. The scan size is 241 × 241 Å^2. The frequency shift is −36 Hz for (a), and −22 Hz for (b). The cross section at the solid lines, the position of which correspond to the line in Fig. 2(a), are also shown. The differences of the average peak height between two kinds of adatoms are 0.56 ± 0.23 and 0.30×0.21 Å, respectively.

that all adatoms in (a) appear in (b), while there are a lot of adatoms, which are resolved only in (b). In addition, between both scans, we obtained another image in which the image contrast suddenly changed from that of (a) to (b). Finally, we think that these differences in the frequency shift and the image contrast are due to the incidental exchange of tip-apex atoms.

Depending on the species of the tip-apex atoms and the surface adatoms, the strength of the chemical bonding force, which primarily contributes to the atomic resolution imaging of NC-AFM, changes. The force between two Si atoms, i.e. the coupling between two dangling bonds, is strong enough for atomic resolution imaging as numbers of results have been shown. In the case of Si–Sb bonding, where a dangling bond and a lone pair forms a chemical bonding, the coupling force becomes weaker, but the chemical bonding force still works. When the both atoms are Sb, the chemical bonding force does not take place any more, but the van der Waals force is dominant in the attractive force. The details of the consideration will be discussed elsewhere [4]. We conclude that Fig. 3(a) and (b) were scanned with an Sb tip and Si tip, respectively. The Si tip can resolve both kinds of adatoms, however, Sb tip cannot resolve Sb adatoms in our experimental condition.

From comparison of the scans in Fig. 3, we can specify atom species of adatoms in Fig. 2 as well. Adatoms, which are resolved in both scans of Fig. 3, are Si, and the others are Sb. Circled adatoms in Fig. 2 are specified as Si adatoms. Since the circles indicate slightly larger adatoms in Fig. 2(a) and darker adatoms in Fig. 2(c), we conclude that we could distinguish Si and Sb atoms through the CPD image of KPFM, while the difference is not decisive in the topography. In addition, for comparison of NC-AFM images like in Fig. 3, occasional exchange of tip-apex atoms must be waited.

At last, we would like to mention a notable feature in Fig. 2(c) that some of the rest atoms on the FH are resolved. Fig. 4(a) is the magnification of the dashed rectangle area in Fig. 2(c), which shows the FH of the $5\sqrt{3} \times 5\sqrt{3}$ structure as illustrated in Fig. 4(b). The image contrast of Fig. 4(a) is inverted to show its contrast clearly. The 4×4 triangle of the rest atoms can be seen and one of them, i.e. leftmost on second bottom line, is imaged as a brighter spot than others. By analogy with appearance of adatoms in Fig. 2(c), we believe that the rest atom is Si while others are Sb. The result suggests the possibility of highly resolved atom distinction using ESF measurement by KPFM.

From Fig. 2(c), we evaluated the surface potential on each adatom, and estimated that the potential at the Si adatom is ∼0.2 eV lower than the potential at the Sb

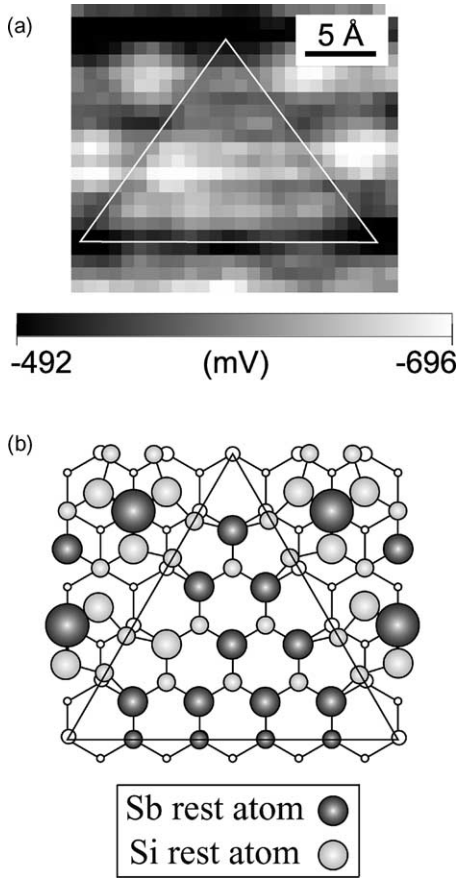

Fig. 4. CPD image (a) of the 4×4 rest atom triangle magnified from Fig. 2(c). The contrast is inverted to look clearly. (b) Alignment of rest atoms on faulted subunit shown in (a).

adatom. This value disagrees with the theoretical work functions of Si and Sb in bulk state. However, it is not incomprehensible because the condition of adatoms is quite different from that of the bulk in the energy level. Similarly, some physical properties for single atoms, such as the ionization energy or the electronegativity, cannot explain the potential difference of our result, although they may give some suggestion. In order to discuss the potential of adatoms, theoretical analysis based on actual surface structure should be performed. Ko et al. [11] performed calculations, and suggested that the energy of the lone pair state of the Sb adatom lay about 0.6 eV below that of the dangling bond state of the Si adatom, which they claimed to lie at the Fermi level. Our result indicates that KPFM on atomic scale does not measure the energy of highest occupied molecular orbital (HOMO) level. Kitamura et al. [8] observed the Au-cluster deposited on an Si surface and reported that the work function measured by KPFM with atomic resolution disagrees with well-known macroscopically measured values, either. (They explain that the CPD image reflects the electron density distribution on the surface.) Imaging mechanism of KPFM on atomic scale is not clearly understood yet.

We point out here the possibility that KPFM measures other kinds of information besides the CPD. At first, we can consider the effect of band bending, which can occur in our case where both the tip and the sample are semiconductor and the quite high bias voltage ($\sim$1 V_{rms}) at low frequency ($\sim$1 kHz) is applied for KPFM measurement. In the principle of KPFM measurement, the dependence of the capacitance between the tip and the sample on the bias voltage is not considered. If the capacitance has the bias voltage dependence due to the band bending, the ESF between the tip and the sample cannot be correctly detected. AC bias voltage has another possibility to induce error signal. When the AC bias voltage is applied, the cantilever oscillation is induced in addition to the resonant oscillation for FM detection method. The additional cantilever oscillation modulates the tip–sample distance with the angular frequency ω, resulting in the modulation of the frequency shift signal at ω. That modulation induces the error to the CPD detection. When the forces with different length scale coexist, such as the short-range chemical bonding and the long-range ESF, the problem is serious. The tunneling current, which can be thought to occur when the atomic resolution is obtained in NC-AFM, could be a problem as well. If the tunneling current shows any spatial inhomogeneity, the associated voltage drop across the tunneling resistance could produce variations of the CPD image. We have not experimentally investigated the possibility of these problems yet. In order to understand KPFM images on atomic scale better, further experiments, as well as the theoretical examination, is required.

In this paper, we observed the Si(1 1 1)$5\sqrt{3} \times 5\sqrt{3}$-Sb surface by an NC-AFM/KPFM system. First, the topography and the CPD was simultaneously measured using KPFM. There was no clear difference

between two kinds of adatoms in topography, but the CPD image showed an obvious difference. Atom species of adatoms were specified by comparison of two NC-AFM images with different tip-apex atoms. An Si tip can image both Si and Sb adatoms, but Sb tip can resolve only Si adatoms. Then we recognized that Si adatoms has a lower surface potential than Sb adatoms. We conclude that atom species of individual adatoms, and in addition rest atoms, could be distinguished by KPFM.

The final goal of this kind of experiment would be the atom identification, which means that arbitrary kind of atom should be specified. In order to achieve the ''atom identification'', a large number of reference data would be required like other successful techniques, such as optical spectroscopy or chromatography, which have accumulated data for various materials. We believe that our result reported here can be the first step to the true ''atom identification.''

Acknowledgements

This work was supported by a Grant-in-Aid for Science Research from the Ministry of Education, Culture, Sports, Science and Technology of Japan and Handai Frontier Research Center.

References

[1] F.J. Giessibl, Science 267 (1995) 68.
[2] S. Kitamura, M. Iwatsuki, Jpn. J. Appl. Phys. 34 (1995) L145.
[3] Y. Sugawara, M. Ohta, H. Ueyama, S. Morita, Science 270 (1995) 1646.
[4] S. Morita, R. Wisendonger, E. Meyer (Eds.), ''Noncontact Atomic Force Microscopy'', Springer, NonoScience and Technology Series, Heidelberg, (2002) pp. 65–68.
[5] M. Nonnenmacher, M.P. O'Boyle, H.K. Wickramasinghe, Appl. Phys. Lett. 58 (1991) 2921.
[6] K. Umeda, K. Kobayashi, K. Ishida, S. Hotta, H. Yamada, K. Matsushige, Jpn. J. Appl. Phys. 40 (2001) 4381.
[7] H. Sugimura, K. Hayashi, N. Saito, A. Takai, N. Nakagiri, Jpn. J. Appl. Phys. 40 (2001) L174.
[8] S. Kitamura, K. Suzuki, M. Iwatsuki, C.B. Mooney, Appl. Surf. Sci. 157 (2000) 222.
[9] K. Okamoto, Y. Sugawara, S. Morita, Appl. Surf. Sci. 188 (2002) 381.
[10] A.A. Saranin, A.V. Zotov, V.G. Lifshits, O. Kubo, T. Harada, M. Katayama, K. Oura, Surf. Sci. 447 (2000) 15.
[11] Y.-J. Ko, K.-H. Park, J.S. Ha, W.S. Yun, Phys. Rev. B 59 (1999) 4588.
[12] C.-Y. Park, T. Abukawa, T. Kinoshita, Y. Enta, S. Kono, Jpn. J. Appl. Phys. 27 (1988) 147.
[13] S. Andrieu, J. Appl. Phys. 69 (1991) 1366.
[14] K.-H. Park, J.S. Ha, W.S. Yun, E.-H. Lee, J.-Y. Yi, S.-J. Park, J. Vac. Sci. Technol. A 15 (1997) 1572.
[15] H.B. Elswijk, D. Dijkkamp, E.J. van Loenen, Phys. Rev. B 44 (1991) 3802.
[16] K.-H. Park, J.S. Ha, W.S. Yun, E.-H. Lee, J.-Y. Yi, S.-J. Park, Phys. Rev. B 55 (1997) 9267.
[17] Y. Kusumi, K. Fujita, M. Ichikawa, Surf. Sci. 372 (1997) 28.